Soft Matter

Cite this: *Soft Matter*, 2011, **7**, 1491

www.rsc.org/softmatter

PAPER

Structural and thermodynamic aspects of the cylinder-to-sphere transition in amphiphilic diblock copolymer micelles

Reidar Lund,*[ab] Vitaliy Pipich,[c] Lutz Willner,[d] Aurel Radulescu,[c] Juan Colmenero[abe] and Dieter Richter[cd]

Received 30th August 2010, Accepted 10th November 2010
DOI: 10.1039/c0sm00894j

The structure of diblock copolymers micelles depends on a delicate balance of thermodynamic forces driving the system towards equilibrium and kinetic factors which limit the systems' exploration of the phase space. The factors governing the morphological transition between cylindrical and spherical micelles are related to a fine balance between entropic forces from chains within the micellar core and corona. In order to understand and control these structures, it is important to gain insight into the fundamental thermodynamic driving forces governing the structure and answer fundamental questions concerning its equilibrium nature. In this work we aim to understand the relationship between thermodynamics and morphological transitions by investigating the detailed structure of a system undergoing a cylinder-to-sphere transition. We focus on the structural properties of micelles constituted of poly(ethylene-*alt*-propylene)–poly(ethylene oxide) (PEP1–PEO1, the numbers indicate the molar mass in kg/mole) diblock copolymers in dimethylformamide (DMF)/water solvent mixtures. This system is ideal for fundamental studies as it represents a classical well-segregated block copolymer micelle system where the interfacial tension can be controlled in detail without significantly changing other thermodynamic properties. Using small-angle neutron scattering (SANS) it is shown that the system undergoes a cylinder-to-sphere transition upon addition of DMF which lowers the interfacial tension. By applying a detailed thermodynamic model we show that both the dependence of the structural parameters with the interfacial tension as well as the morphological transition can be quantitatively understood. The transition itself is governed by the interfacial tension which dictates the stretching of chains within both corona and core. At high interfacial tensions (in water-rich solutions) discrepancies between structural data and predictions from the thermodynamic model are observed. A qualitative comparison with some preliminary results on the chain exchange kinetics in the system show that these deviations coincide with the region where this equilibration mechanism is not active, *i.e.* when the kinetics are frozen at high interfacial tensions.

1 Introduction

Block copolymers in selective solvents classically form either lamellar, cylindrical or spherical micelles depending on the interaction parameters, temperature and molecular weight,[1–5] although in some cases vesicular structures are also reported.[6] As a consequence of the usually preferred spontaneous curvature of swollen coronal chains in polymeric systems, the most commonly observed are spherical micelles. For block copolymers with a larger soluble block than insoluble part, spherical micelles are indeed practically always formed.[9,10] Lamellar aggregates are not readily observed in block copolymer solutions as these are likely to phase separate out of the solution or rather form curved analogous like vesicles.[6] However while, vesicles are rather rare and formed in a narrow parameter range,[6] cylindrical micelles are a much more frequent observation.[9,11–14] This is usually the case in symmetric block copolymers where the core dimension is larger than the corona ("crew-cut" micelles).[5] This is reflected in earlier findings of micelles formed by a series of symmetric poly(ethylene-*alt*-propylene)–poly(ethylene oxide) (PEP–PEO) in water, where it was found that cylinders were favoured for low overall molecular weights characterized by large aggregation numbers (core radii) and small corona, while spherical micelles were formed for higher molecular weights where the core–corona dimensions are more balanced.[11] In a work by Bang *et al.*[13] and Abbas *et al.*,[14] transitions between spherical, cylindrical and even vesicular micelles were induced by changing the spontaneous curvature of the micelles *via* the solvent quality towards the

[a]*Donostia International Physics Center, Paseo Manuel de Lardizabal 4, 20018 Donostia-San Sebastián, Spain. E-mail: reidar_lund@ehu.es*
[b]*Centro de Física de Materiales (Centro Mixto CSIC-UPV/EHU), Paseo Manuel de Lardizabal, 3, 20018 Donostia-San Sebastián, Spain*
[c]*Jülich Center for Neutron Science (JCNS) at FRM-II, Lichtenbergstr. 1, 85747 Garching, Germany*
[d]*Forschungszentrum Jülich GmbH, Institute of Solid State Research, 52425 Jülich, Germany*
[e]*UPV/EHU: Departamento de Física de Materiales, Paseo Manuel de Lardizabal, 3, 20018 Donostia-San Sebastián, Spain*

corona forming block. Interestingly, in the case of the poly(styrene)–poly(dimethylsiloxane) (PS–PDMS) in phthalates studied by Abbas *et al.*[14] and the poly(styrene)–poly(isoprene) (PS–PI)/heptane system by La Rue *et al.*,[12] the micellar transitions were found to be thermally reversible indicating that the systems are in equilibrium. A similar observation from spherical to cylindrical morphology was observed in another block copolymer system where the solvent quality to the corona block was changed from good to theta-like by decreasing the temperature although here this was accompanied by a crystallization of the core polymer.[15] This type of morphological change, induced by changing the spontaneous curvature of the corona, is completely analogues to that in surfactant micelles which is usually driven by reduced head-group interactions *e.g.* upon salt addition, temperature change *etc.*[16] In contrast, polymeric systems may exhibit transitions that are driven by forces of purely entropic origin, *i.e.* chain stretching and the consequent elastic energy of the core.[3,4,17,18] This is well-established in the literature available for block copolymer melts where both theory[3,17] and experiment[19–21] show that the sphere-to-cylinder transition is determined by a delicate balance between chain stretching and interfacial energy. However, an important difference between block copolymer melts and solutions is that as a consequence of excluded volume effects, the transition region is moved from asymmetric block compositions in melts (typically 20%) to roughly symmetric compositions in solution.[5,18] For block copolymer solutions, the theoretical work by Zhulina *et al.*,[5] demonstrates that the small but non-negligible elastic chain stretching in the core constitutes the main thermodynamic driving force for the formation of cylindrical micelles. In a comparative study between experimental and theory, La Rue *et al.*[5,12] found that for a series of thermoresponsive poly(styrene)–poly(isoprene) (PS–PI) block copolymers theory could reproduce both the molecular weight dependence of the structural parameters and phase boundaries as well as the temperature dependence. Apart from these works which consider thermoresponsive swollen micelles in organic solvents, there is a lack of studies where morphological transitions in block copolymer systems are addressed with both detailed structural data and thermodynamic model.

In addition to thermodynamic factors, kinetics can play a decisive role on the final structures in block copolymer systems.[7,8] In order to achieve full equilibration, the system must be in dynamic equilibrium, *i.e.* the chains must continuously exchange between the micelles. It has been shown in a series of time-resolved small-angle neutron scattering (SANS) experiments[22–26] that the kinetics of chain exchange, is intrinsically extremely slow and can be completely frozen in aqueous solutions[22–24] as a consequence of high interfacial tensions. It has also been shown in a recent synchrotron small-angle X-ray scattering (SAXS) experiment[27] with millisecond time resolution that this chain exchange mechanism is the predominant growth mechanism for block copolymer micelles at least in micelles with extended coronas. Eisenberg and coworkers demonstrated in a series of experiments that the structure of block copolymer micelles may depend on the preparation method which may be used to create various non-equilibrium structures.[7] Zhang and Eisenberg[8] also showed that both kinetic and thermodynamic aspects are important in morphological transitions with high water contents. Hence it is important to keep in mind both kinetic as well as thermodynamic aspects with respect to the structural properties of the system. In an earlier work such a combined structural and thermodynamic investigation where the kinetics were discussed was done in a system of weakly segregated spherical micelles formed by a symmetric poly(styrene)–poly(butadiene) diblock copolymer in a homologous series of *n*-alkanes.[28] Here it was found that the micelles are in kinetic equilibrium and the aggregation behaviour of the spherical micelles could be nicely described with a mean-field thermodynamic model. However, there is a distinct lack of studies addressing structural, thermodynamic and kinetic issues in the context of the cylinder to sphere transition.

In this work we consider micelles formed by a model amphiphilic block copolymer system and follow the detailed structural properties of the micelles across the morphological transition using small-angle neutron scattering (SANS). The structural parameters and transitions are quantitatively discussed in terms of a detailed thermodynamic model. The studied micelles are formed by symmetric PEP1–PEO1 (the numbers indicate the molecular weight in kg/mole) in solvent mixtures of water and *N*,*N*-dimethylformamide (DMF). As shown in previous publications, the composition of the DMF–water mixtures represents a convenient tuning parameter for the interfacial tension towards PEP which may be varied between $\approx$ 46 and 8 mN m^{-1} representing the values in pure water and DMF respectively.[29] The results show that PEP1–PEO1 exhibits a clear transition from cylindrical to spherical micelles upon addition of DMF. The aim of this study is to scrutinize in detail the structural properties of block copolymer micelles undergoing cylinder to sphere transitions and discuss the thermodynamic driving force responsible for this transition. Special attention is given to the non-equilibrium/equilibrium properties of the final micelles in terms of their chain exchange kinetics. Although, a thorough discussion of the kinetic mechanism *etc.* will be presented in a forthcoming publication, we will briefly discuss the equilibration ability of the system in light of some of these recent preliminary results.

2 Theoretical background

2.1 Thermodynamic models

In the usual thermodynamic picture of A–B block copolymer micelles, the aggregation is governed by three main components: the interfacial energy between core and solvent, F_{int}; the elastic energy of the chains in the core, F_{core}; and the free energy associated with the chains in the corona, F_{corona}. The free energy *per* chain in units of $k_{\mathrm{B}}T$ (k_{B} is the Boltzmann constant and T the temperature) for spherical or cylindrical block copolymer micelles can be written as:[3]

$$F_{\mathrm{micelle}} = F_{\mathrm{corona}} + F_{\mathrm{core}} + F_{\mathrm{int}} \quad (1)$$

The interface contribution can be calculated in a straight forward way and equals the area of the micellar core times the interfacial tension, γ. The contributions can be written as:

$$F_{\mathrm{int}} = \frac{A_j \cdot \gamma}{P \cdot k_B T} \begin{cases} A_j = 4\pi R_{\mathrm{c}}^2 & \text{Spheres} \\ A_j = 2\pi R_{\mathrm{c}} L & \text{Cylinders} \end{cases}, \quad (2)$$

$$I(Q)_{\mathrm{CS}}^{\mathrm{calc}} = \frac{\phi}{PV_{\mathrm{PEP-PEO}}}\left(\begin{array}{c}\Delta\rho_{\mathrm{c}}^2P^2\cdot V_{\mathrm{PEP}}^2\cdot A(Q)_{\mathrm{c}}^2+\Delta\rho_{\mathrm{sh}}^2P\cdot\left(P-F(0)_{\mathrm{blob}}\right)\cdot V_{\mathrm{PEO}}^2\cdot A(Q)_{\mathrm{sh}}^2\\ +2\Delta\rho_{\mathrm{c}}\cdot\Delta\rho_{\mathrm{sh}}P^2\cdot V_{\mathrm{PEO}}\cdot V_{\mathrm{PEP}}\cdot A(Q)_{\mathrm{c}}A(Q)_{\mathrm{sh}}+V_{\mathrm{PEO}}^2\Delta\rho_{\mathrm{sh}}^2\cdot F(Q)_{\mathrm{blob}}(Q)\end{array}\right) \quad (6)$$

where γ is the interfacial tension and R_{c} the core radius. The aggregation number P can be related to other micellar parameters assuming a compact (solvent-free) core: $P = \pi R_{\mathrm{c}}^2L/(V_{\mathrm{PEP}}/N_{\mathrm{Avo}})$ and $P = 4\pi R_{\mathrm{c}}^3/(3\cdot V_{\mathrm{PEP}}/N_{\mathrm{Avo}})$ for cylinders and spheres respectively. Here V_{PEP} is the molar volume of the insoluble PEP block and N_{Avo} is Avagadro's number.

For the corona contribution we will follow the approach by Zhulina *et al.*[5] who showed that one may write this contribution as:

$$F_{\mathrm{corona}} = C_F\int_{R_{\mathrm{c}}}^{R_{\mathrm{c}}+D} s(r)^{-1/2}\mathrm{d}x;\begin{cases} s(r) = s_0\left(\frac{r}{R_{\mathrm{c}}}\right)^2 & \text{Spheres}\\ s(r) = s_0\frac{r}{R_{\mathrm{c}}} & \text{Cylinders}\end{cases}, \quad (3)$$

where $s(r)$ is a function that describes the radial dependence of the grafting density, s (the area available per chain) which on the core surface ($r = 0$) is equal to $s_0 = 4\pi R_{\mathrm{c}}^2/P$ and $s_0 = 2\pi R_{\mathrm{c}}\cdot L/P$ for spherical and cylindrical micelles respectively. After some calculus Zhulina *et al.* showed that the analytical expressions of F_{corona} can be written as:

$$F_{\mathrm{corona}} = \begin{cases} \frac{\nu C_F R_{\mathrm{c}}}{\sqrt{s}}\ln\left(1+\frac{l_{\mathrm{PEO}}C_H N_{\mathrm{PEO}}\left(s/l_{\mathrm{PEO}}^2\right)^{(\nu-1)/2\nu}}{\nu R_{\mathrm{c}}}\right) & \text{Spheres}\\ \frac{2C_F R_{\mathrm{c}}}{\sqrt{s}}\left[\left(1+\frac{(1+\nu)\cdot l_{\mathrm{PEO}}C_H N_{\mathrm{PEO}}\left(s/l_{\mathrm{PEO}}^2\right)^{(\nu-1)/2\nu}}{2\nu R_{\mathrm{c}}}\right)^{\nu/(\nu+1)}-1\right] & \text{Cylinders}\end{cases} \quad (4)$$

Here C_F and C_H are numerical prefactors, l_{PEP} and l_{PEO} the effective segment lengths of PEP and PEO. N_{PEP} and N_{PEO} denote the respective number of repeat units, ν is the excluded volume parameter controlling the conformation of the chain. In a good solvent ν takes the well known value 0.588.

F_{core} corresponds to the elastic energy associated with stretching the chains beyond their unperturbed end-to-end distance to the radius of the core. This contribution was carefully worked out for various geometries by Semenov[3] who took into account the fraction of chain-ends needed to effectively fill the core. The results are:

$$F_{\mathrm{core}} = k_j\cdot\frac{R_{\mathrm{c}}^2}{R_{\mathrm{ee}}^2};\begin{cases} k_j = \frac{\pi^2}{16} & \text{Spheres}\\ k_j = \frac{3\pi^2}{80} & \text{Cylinders}\end{cases} \quad (5)$$

where R_{c} is the core radius and $R_{\mathrm{ee}} \approx N_{\mathrm{PEP}}^{1/2}l_{\mathrm{PEP}}$ is the unperturbed (bulk) end-to-end radius of gyration of the core forming polymer. The units are in $k_{\mathrm{B}}T$ as before.

In the analysis the set of expressions constituted by eqn (1)–(5), was numerically minimized with respect to R_{c} (GNU Scientific Library) and iteratively fitted to the experimental data.

2.2 Small-angle scattering: models

In order to extract accurate and detailed structural information, the data were analysed using form factors calculated from core–shell scattering model with explicit density profiles. For cylindrical or spherical micelles, such scattering functions have the following generic form:[30,31] where $A(Q)_{\mathrm{c}}$ and $A(Q)_{\mathrm{sh}}$ are the scattering amplitude of core and shell (corona) respectively, V_{i} is the molecular volume of the PEP or PEO block, $\Delta\rho_{\mathrm{sh}} = (\rho_{\mathrm{PEO}} - \rho_0)$, $\Delta\rho_{\mathrm{c}} = (\rho_{\mathrm{PEP}} - \rho_0)$ and $F(Q)$ is the effective scattering from the PEO polymers constituting the corona ("blob scattering"). ϕ is the volume fraction of block copolymer.

The scattering amplitude for the core can be written as:

$$A(Q)_c = \begin{cases} \frac{3(\sin(Q\cdot R_{\mathrm{c}}) - Q\cdot R_{\mathrm{c}}\cos(Q\cdot R_{\mathrm{c}}))}{(Q\cdot R_{\mathrm{c}})^3}\cdot DW(Q,\sigma) & \text{Spheres}\\ \frac{\sin(Q\cdot L\cos(\alpha)/2)}{Q\cdot L\cos(\alpha)/2}\frac{2J_1(Q\cdot R_{\mathrm{c}}\sin(\alpha))}{Q\cdot R_{\mathrm{c}}\sin(\alpha)}\cdot DW(Q,\sigma) & \text{Cylinders}\end{cases} \quad (7)$$

$DW(Q,\sigma) = \exp(-Q^2\sigma^2/2)$, where σ is the Gaussian width of the core–shell interface. R_{c} denotes the core radius, L the length of the cylinder, and α the angle between the cylinder axis and the scattering vector, $\mathbf{Q}$.

$$A(Q)_{sh} = \begin{cases} \frac{1}{C}\int_0^\infty 4\pi r^2 n(r)\frac{\sin(Qr)}{Qr}\mathrm{d}r\cdot DW(Q,\sigma) & \text{Spheres}\\ \frac{1}{C}\int_{R_{\mathrm{c}}}^\infty 2\pi r\cdot n(r)J_1(Q\cdot r\sin(\alpha))\mathrm{d}r\cdot DW(Q,\sigma) & \text{Cylinders}\end{cases} \quad (8)$$

C is a normalization constant obtained by integration the density profile over the volume and $J_1(x)$ is the Bessel function of first order. The density profile can conveniently be chosen to have the following generic form:

$$n(r) \sim \frac{1}{1+\exp((r-R_{\mathrm{m}})/(\sigma_m R_{\mathrm{m}})} \quad (9)$$

where σ_{m} is the relative width of the micellar surface and R_{m} is the mean radius of the micelle.

As shown by Pedersen and Svaneborg the scattering from the swollen PEO polymer chains in the corona—the "blob scattering"—can be written as:[30,31]

$$F(Q) = \frac{P(Q)_{\mathrm{chain}}}{1+\hat{\nu}\cdot P(Q)_{\mathrm{chain}}} \quad (10)$$

where $P(Q)_{\mathrm{chain}}$ is the form factor of a polymer chain, $\hat{\nu}$ is an effective virial type parameter that scales with the effective concentrations of corona chains.[30,31] The form factor of a polymer chain can be conveniently approximated by the following equation suggested by Beaucage[32] valid for arbitrary chain statistics:

$$P(Q)_{\mathrm{chain}} = \exp\left(-Q^2R_{\mathrm{g}}^2/3\right) + \left(d_{\mathrm{f}}/R_{\mathrm{g}}^{d_{\mathrm{f}}}\right)\Gamma(d_{\mathrm{f}}/2)\left(\frac{\left(\mathrm{erf}\left(Q\,k\,R_{\mathrm{g}}/\sqrt{6}\right)^3\right)}{Q}\right)^{d_{\mathrm{f}}} \quad (11)$$

where d_f is the fractal dimension. For mass fractals: $1 \leq d_f \leq 3$, for polymers in a good solvent a typical value is 1.7. k is a numerical constant equal to 1.06.[32]

In order to take into account finite interference effects, a virial expansion was used which after ignoring higher-order terms can be written as:

$$I(Q)^{\text{calc}}_{\text{mic.}} = \phi \frac{I(Q)^{\text{calc}}_{CS}}{1 + 2I(Q)^{\text{calc}}_{CS} \cdot A_2 \phi} \quad (12)$$

where A_2 is an effective virial coefficient. Finally, the calculated intensity was convoluted with the resolution function estimated using the approach by Pedersen *et al.*[33]

3 Experimental section

3.1 SANS experiments

The static SANS experiments were performed at the KWS2 instrument at the FRM2 reactor in Garching, Germany. The data were collected using a wavelength of $\lambda = 4.5$ Å and in some cases 12 Å, and two detector distances of 8 and 2 m in order to cover an extended range of wave vectors, Q, ($Q = 4\pi\sin(\theta/2)/\lambda$, where θ is the scattering angle). The collimation was held fixed to 8 m in order to improve the resolution as well as to reduce the flux and thereby avoiding significant dead time corrections of the detector. The spread in wave length, $\Delta\lambda/\lambda$ was 20%. Detector sensitivity corrections were made using Plexi glass which was also used as secondary standard. The primary standard used was vanadium. Empty cell scattering and the background signal arising from electronic noise, gamma radiation and fast unmoderated neutrons were subtracted using standard procedures. The background noise was determined using boron carbide to block the primary beam. All background subtraction was done directly pixel by pixel on the two-dimensional detector intensity image. After radial averaging the intensities were treated for dead time effects which then finally give the absolute normalized macroscopic differential scattering cross-sections, $\frac{d\Sigma}{d\Omega}(Q)$.

All data reduction, calibration and analysis was performed using the QtiKWS program package.[36]

3.1.1 Polymer synthesis. The PEP1–PEO1 block copolymer was synthesized by anionic polymerization basically following the two step procedure outlined in ref. 35. This procedure involved the synthesis of the OH-end functionalized polyisoprene which was subsequently saturated with hydrogen to the corresponding PEP1–OH polymer by means of a conventional Pd/$BaSO_4$ catalyst. The PEP1–OH polymer was transferred to a macroinitiator with potassium as the counterion serving as the initiator for the polymerization of ethylene oxide. The number average molecular weights, M_n, of both blocks were determined by ^{1}H-NMR using the *t*-butyl group of the initiator as an internal reference. For PEP $M_n(PEP) = 1200$ g mol^{-1} and for PEO $M_n(PEO) = 1500$ g mol^{-1} was obtained. This corresponds to an average degree of polymerization of $N_{PEP} = 17$ and $N_{PEO} = 34$. The polymers were further characterized by size exclusion chromatography (SEC) in tetrahydrofuran/dimethylacetamid (90/10) as eluent at 40 °C. The chromatogram of the final PEP1–PEO1 block copolymer shows a single peak with no visible sign of PEP1 homopolymer. Using polystyrene standards the polydispersity, M_w/M_n, was determined to be 1.06 for the PEP block and 1.04 for the final block copolymer.

3.1.2 Sample preparation and calculation of scattering length densities. The solvents used in this study were both deuterated in order to obtain full contrast to the fully protonated PEP1–PEO1 polymer. D_2O (Aldrich, 99.8% D), and DMF-d_7 (Chemotrade, Leipzig 99.5% D) were used as received without further purification. The densities of the solvent mixtures, d_{mix} were measured using a Anton Paar DMA 5000 instrument in order to calculate the scattering length density of the solvent, ρ_0, according to:

$$\rho_0 = \frac{N_{Avo} \sum_i x_i b_i}{\sum_i x_i M_i} \cdot d_{\text{mix}} \quad (13)$$

where x_i is the molar fraction, b_i the scattering length, and M_i is the molecular weight of the components.

For the polymers we used the calculated scattering length densities given in ref. [29] for 20 °C: $\rho_{PEP} = -3.01 \times 10^9$ cm^{-2} and $\rho_{PEO} = 6.35 \times 10^9$cm^{-2}. An attempt to use the reported solution densities of PEO of 1.2 g cm^{-3} [34] instead of the bulk density of $d_{PEO} = 1.125$ g cm^{-3} for the calculation of ρ_{PEO} did not influence the results in any significant way as the contrasts between the micelles and the deuterated solvent mixture are in all cases very large. In all cases the solutions were made by direct dissolution of the polymer powder in the premixed D_2O/DMF-d_7 solvent mixtures. The standard sample preparation involved dissolution of the samples by heating at 70 °C for approximately 30 min and subsequent equilibration by shaking over night at room

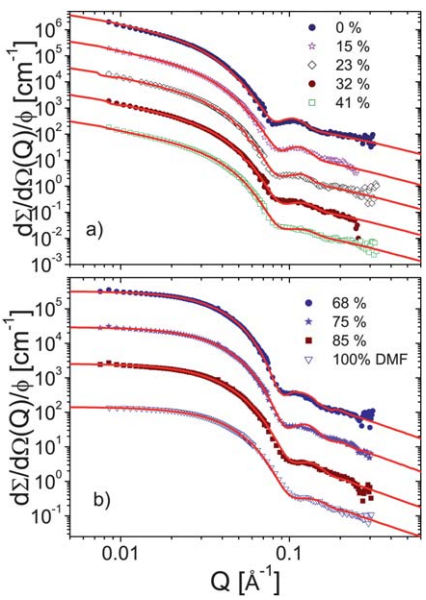

Fig. 1 Small-angle neutron scattering (SANS) data of hPEP1–hPEO1 in various d-DMF/D_2O mixtures of a) 0–41% d-DMF and b), 68–100% d-DMF. The solid lines represent the best fit using either a) cylindrical or in b) spherical core–shell form factor models with detailed Fermi–Dirac density profiles. For better visibility the data have been shifted vertically using the following multiplication factors: a); 100, 10, 1, 0.1, 0.01 and in b); 100, 10, 1, 0.1 (from top to bottom).

temperature. Thus completely transparent homogeneous solutions were obtained. It was qualitatively observed that solutions containing cylindrical micelles were more viscous than those with spherical aggregates. In the transition region between cylinders and spheres it turned out that the thermal treatment during the sample preparation effects the morphology. In these cases different preparation methods were applied. This will be discussed later under "Results and Discussion" in more detail.

4 Results & discussion

4.1 Morphological transition induced by addition of DMF

The SANS scattering curves of PEP1–PEO1 are shown in Fig. 1 for various d-DMF/D_2O mixtures. As is evident from Fig. 1a), the scattering in the low-Q range follows a characteristic Q^{-1} behaviour which indicates that long cylindrical or worm-like micelles are formed in low-DMF mole fractions up to at least 41% d-DMF. At higher d-DMF fractions in the range above approximately 50% (Fig. 1b)), the data shows a Guinier-like plateau in the double logarithmic presentation which thus might indicate spherical micelles.

In order to extract accurate structural information, we employed the detailed core-shell scattering models described in Section 2.2. For the cylindrical micelles, it turned out that the data could be described by a core–shell model with essentially compact homogeneous density profile of the corona since σ_m was found to be ≈ 0. In all cases the cylinder length was not found to be resolved within the accessible Q-range of SANS. Instead a continuous power-law behaviour close to Q^{-1} rather than a cross-over to a Guinier-like plateau at low Q is found. However, in some cases where the Q-range was extended up to the lowest Q using the $\lambda = 12$ Å option, some depression in the forward scattering with respect to the cylinder form factor occurred. As attempts to reduce the cylinder length to fit the data failed, we interpret this effect as interference effects between micelles, *i.e.* repulsive structure factor effects. As the concentration of polymers is low (0.5–1.0%) and thus in the dilute regime, we can then use a virial expansion according to eqn (12). The cylinder length was consequently fixed to the (rather arbitrary number) $L = 1000$ Å which for the purpose can be considered "infinitely" long in this Q-range. The resulting fit curves are represented by the solid lines in Fig. 1. The extracted final fit parameters are summarized in Table 1 for the cylindrical micelles.

Above about 50% d-DMF, a change in the scattering curves is observed. This is prominent in the data of 51% d-DMF solution shown in Fig. 2. Here a fit using cylindrical micelles fails completely. However, as shown in Fig. 2 a spherical core–shell model (dotted lines) does not seem to satisfactorily describe the data either. Here deviations are seen, especially at the lowest Q-vectors. In order to take into account an excess scattering at low Q, we considered a coexistence model where both spherical and cylindrical micelles exist in solution. Such model can be written as:

$$I(Q)^{\text{calc}}_{\text{sphere-cyl}} = f_{\text{spheres}} \cdot I(Q)^{\text{calc}}_{\text{spheres}} + (1 - f_{\text{spheres}}) \cdot I(Q)^{\text{calc}}_{\text{cyl}} \quad (14)$$

where f_{spheres} is the fraction of spherical micelles; $I(Q)^{\text{calc}}_{\text{spheres}}$ and $I(Q)^{\text{calc}}_{\text{cyl}}$ can be calculated using the appropriate scattering amplitudes and intensity constructions represented by eqn (6)–(12) above in Section 2.

As demonstrated by the solid line in Fig. 2, the coexistence model works nicely giving a $f_{\text{spheres}} = 0.89$, *i.e.* the spheres coexist with approximately 10% cylindrical micelles. The structural parameters corresponding to the small amount could not be deduced with high accuracy and were fixed to the values $R_c = 39$ Å and $R_m = 88$ Å which are the values obtained if no thermal treatment is applied (see subsequent section).

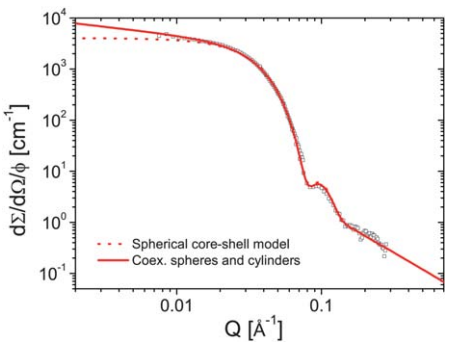

Fig. 2 Small-angle neutron scattering (SANS) data corresponding to the micellar solution in 51% d-DMF in the solvent mixture. The sample was heated to 70 °C for 30 min and then allowed to be shaken at room temperature over night. The dotted lines displays a fit using a pure spherical core–shell model. The solid line represents the best fit using a linear combination of the intensity of about 90% spherical and 10% cylindrical micelles.

Table 1 Structural parameters extracted from core–shell model fits of the cylindrical micelles in various d-DMF/D_2O compositions

% d-DMF	R_m/Å	R_c/Å	D_{corona}/Å	s_0/Å^2	A_2/10^{-6}mole cm^{-3}	R_g/Å	σ_{int}/Å	$\hat{\nu}$
0	110 ± 11	48 ± 2	62	100	—	16 ± 2.2	10.1 ± 2	0.2
0[a]	110 ± 10	48 ± 2	62	100	5.2	17.6 ± 2	9.5 ± 5	0.7
0[b]	106 ± 10	47 ± 2	59	101	6.2	17.5 ± 2	9.9 ± 3	0.1
15	100 ± 29	45 ± 3	56	107	—	19 ± 3	9.5 ± 2	0.4
23	88 ± 15	44 ± 2	45	110	—	17 ± 8	9.8 ± 2	0.2
32	87 ± 30	42 ± 2	45	114	—	17 ± 8	10.4 ± 2	0.3
41	88 ± 8	43 ± 3	45	112	3.3	17 ± 4.7	9 ± 2	0.1
51[c]	89.9 ± 2	39 ± 2	51	121	11	16 ± 2	11 ± 2	0.6

[a] Initial state at 20 °C before heat treatment. [b] at 20 °C after a heat treatment at 70 °C for 20 h. [c] Sample prepared by direct dissolution without any heat treatment.

The data above 51% d-DMF could be well described using the spherical core–shell model described in Section 2. In all cases it was necessary to include a slight smearing of the corona profile where σ_m was found to be close to 10–20%. In all cases the model description taking only into account micellar scattering neglecting free (unaggregated) chains worked well. The only exception was the solution in 100% d-DMF, where the micellar form factor alone gave poor fits. Here it was necessary to include the scattering from single chains. This was achieved in a straightforward manner using a linear combination of the two contributions:

$$I(Q)^{calc}_{mic.-chains} = f_{mic} \cdot I(Q)^{calc}_{mic.} + (1 - f_{mic}) \cdot I(Q)^{calc}_{chain} \quad (15)$$

here we can write $I(Q)^{calc}_{chain} = \phi \cdot V_{PEP-PEO} \cdot (\rho_{PEP-PEO} - \rho_0)^2 P(Q)_{chain}$ where $P(Q)_{chain}$ is given by eqn (11).

For simplicity and in order to avoid an unnecessary amplification of free parameters, the same R_g for the chains dissolved in solution and in the corona was used. Using this description, perfect fits could be obtained where we get $f_{mic} = 0.71$. Since $f_{mic} = 1 - cmc/\phi$ and $\phi = 1.04\%$, this translates to a critical micelle concentration, *cmc*, of about 0.37%. However given the lack of a systematic concentration series, this parameter remains uncertain. In any case an accurate determination and investigation of the *cmc* is beyond the scope of this paper where the focus is on the micellar structure. Fitted parameters for the spherical micelles are listed in Table 2.

The corona thickness (defined by $D_{corona} = (1 + \sigma_m) \cdot R_m - R_c$) is found to decrease from about 60 Å to 40 Å for the cylindrical micelles but then again increases from about 20 to 26 Å for the spherical micelles. This quantity can be compared with the value R_g measured in water by light scattering ($R_g = 0.215 \cdot M_{PEO}^{0.588}$ given in ref. 37) and the value expected in bulk: $R_g = \sqrt{N_{PEO}/6} l^{mon}_{PEO}$. Using an estimated monomer length of $l^{mon}_{PEO} = 3.8$ Å and $M_{PEO} = 1500$ g mol^{-1}, we obtain 16 and 9 Å respectively. Using the relation $R_{ee} = \sqrt{6} R_g$ which is strictly valid only for Gaussian statistics, this translates to an end-to-end vector of $R_{ee} = 39$–22 Å. Comparing with the data, we see that the values for the cylindrical micelles indicate that in all cases the chains are strongly stretched. For the spherical micelles it seems like the corona is collapsed almost to the bulk value at 51% solution and then is progressively extended at higher DMF contents. This apparently peculiar behaviour can be rationalized with small but measurable change in the solvent quality towards PEO in DMF–water mixtures. In ref. 29 we found that the solvent quality manifested by the second virial coefficient, A_2 initially decreases and displays a minimum before it increases again. Although prone to systematic errors associated with uncertainties in background subtraction, the same behaviour is indicated in the values for R_g extracted directly from the fits. This quantity seems to decrease very slightly from pure D_2O ($\approx$ 18 Å) towards about 15 Å in 68% d-DMF, before increasing again and takes values of about 19 Å in 100% d-DMF. Interestingly, such behaviour also seen in ref. 29 for linear chains in terms of A_2, has been rationalized in a recent theoretical work. Here a minimum in the solvent quality for a mixture of two good solvents is attributed to competing hydrogen bonding.[38]

It is important to point out that the micellar corona is generally significantly more extended in cylindrical than the spherical micelles. The same is reflect in the area per chain, s_0. The quantity is significantly lower for cylindrical than for spherical micelles. Hence in the corona of the cylindrical micelles the chains need to stretch out more due to the lower available volume which thus increases the free energy of the micelles. This, together with the contribution from the elastic chain stretching in the core, in fact represent the balance of forces that drives the morphological transition. We will come back to the transition later in the article where we discuss the results in terms of a detailed quantitative thermodynamical model.

4.2 Thermal stability and effect of sample treatment

All results presented in the previous section were based on samples prepared as described in the Experimental Section by dissolving the polymer at 70 °C for 30 min and equilibrating the solution by shaking over night. Since equilibration of block copolymer micelles is slow and path dependent morphologies (*e.g.* see the work by Eisenberg and coworkers[8]) may occur, we investigated the influence of the preparation method, in particular the thermal treatment on the final structure for two selected samples.

The two samples investigated were PEP1–PEO1 in 0% (pure D_2O) and 51% d-DMF in the solvent mixture which are well inside the cylindrical regime and just in the transition zone between cylinders and spheres respectively. The samples were first dissolved and equilibrated under shaking for one night without any heat treatment and measured. Thereafter the samples were heated at 70 °C for 20 h and remeasured after cooling down to room temperature. A comparison of the resulting scattering curves is shown in Fig. 3.

As seen the effect of the thermal treatment obviously depends on the solvent composition. The morphology of the micellar solution in pure water is not affected and can be satisfactorily fitted with a cylindrical core–shell form factor with minor

Table 2 Micellar parameters extracted from the detailed fit using a spherical core–shell form factor

% d-DMF	P	f_{mic}	R_m/Å	σ_m	R_c/Å	D_{corona}/Å	s_0/Å^2	R_g/Å	σ_{int}/Å	$\hat{\nu}$
51[a]	198 ± 3	1	63 ± 4	0.1	50 ± 3	20	159	22 ± 3	5.4	0.03
51[b]	173 ± 2	1	63 ± 5	0.1	48 ± 1.5	22	166	10 ± 2	5	1.87
68	160 ± 2	1	64 ± 2	0.12	47 ± 3	26	170	15 ± 6	0	0.46
75	148 ± 2	1	57 ± 5	0.19	45 ± 3	22	175	14 ± 4	2.2	0.03
86	135 ± 2.6	1	58 ± 5	0.2	44 ± 2	26	180	14 ± 4	2.6	0.12
100[c]	113 ± 3	0.6 ± 0.1	61 ± 6	0.1	41.6 ± 3	26	191	18.6 ± 2	1.3	0.19

[a] Coexistence fit with cylindrical and spherical micelles. Parameters for the cylinder part: $R_c = 39$ Å and $R_m = 88$ Å. [b] Same samples as the 51% solution in Table 1 after 12 h at 70 °C. [c] Coexistence fit using a linear combination of scattered intensities from micelles and dissolved linear chains.

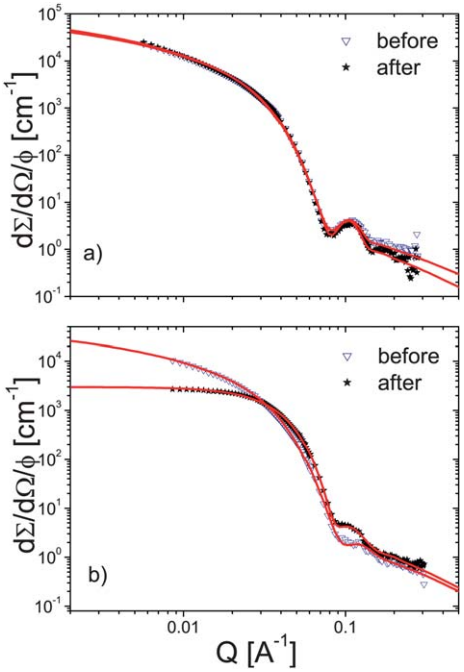

Fig. 3 Small-angle neutron scattering (SANS) data of the hPEP1–hPEO1 in a) D_2O and, b) 50% d-DMF in the solvent mixture before and after a thermal treatment of 20 h at 70 °C. The solid lines represent the best fit using either cylindrical or spherical core–shell form factor models.

changes in the fit parameters. The structure of the 51% d-DMF solution on the other hand strongly depends on the preparation. While clearly defined cylindrical micelles are formed without heat treatment, a transition from cylinders to spheres upon heating is observed. This is consistent with the results shown in Fig. 2, where a brief heat treatment at 70 °C for 30 min is enough to create a mixture of predominantly about 90% spherical micelles. This transition seems to be irreversible as the spherical micelles were observed to be stable at least within the experimental time range (days). Similar behavior was observed in a test experiment where a solution of spherical micelles at 69% d-DMF was diluted with water to give a final 51% d-DMF composition (data not shown). Here, a morphological transitions was not observed either—not even in a time scale of about a month.

Hence while the cylinders formed in pure D_2O seem to be at least thermally stable, the cylinders in 51% d-DMF which are close to the region of transition seem to be metastable and readily decompose into spherical micelles. How this transition proceeds in time, *i.e.* kinetic studies is outside the focus of this paper and will be subject of a future publication. The discussion whether the micelles in water are thermodynamically stable or kinetically trapped, we postpone to the subsequent sections.

4.2.1 Comparison with a thermodynamic model. The morphological map and a representation of the micellar core radius, R_c and the surface area per chain s_0 are given as a function of d-DMF content in Fig. 4.

As shown in the previously presented fit results (Table 1 and 2), the aggregation number and consequently the micellar core radius decreases with the d-DMF content. This effect can be intuitively understood in terms of the reduction in interfacial tension which allows the system to decrease its interfacial energy

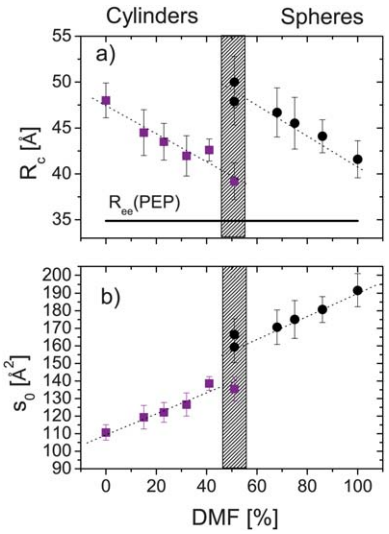

Fig. 4 Morphological map of the system in terms a), of the extracted core radii R_c and; b) area per chain at the interface s_0 at various d-DMF/D_2O compositions. The horizontal line in a) represents the value for the unperturbed end-to-end radius of PEP. The dotted lines are meant as a guide for the eye only.

and consequently smaller micelles to form. As mentioned before, the area per chain on the interface is smaller in cylindrical micelles than for spherical micelles. This is shown in Fig. 4 where it is evident that s_0 makes a discrete jump in the transition zone.

With these features we can qualitatively understand the transition between cylindrical and spherical micelles. The interfacial energy will try to maximize the surface area by increasing the core radius. This is counteracted by increasing stretching of chains in the core and the corona. Since a cylindrical micelle always will have a smaller equivalent core radius than a spherical one†, cylindrical micelles are favored to minimize the extension of the chains in the core, and then minimize the elastic free energy. This is illustrated graphically in Fig. 4 where also the calculated unperturbed end-to-end radius of PEP, R_{ee}^{PEP} is plotted. As seen the measured core radii of the cylinders are always smaller and closer to the unperturbed PEP radius as compared to the equivalent spherical micelles. Spherical micelles will be favoured when the coronal free energy is dominant as the chains will have more available space (larger s_0). Hence with large interfacial tensions (water-rich solvents), micellar cores will be large and the core free energy dominates which thus favours cylindrical micelles. At lower interfacial energies, the core free energy contribution will decrease and the corona free energy will favour spheres. Hence, in this qualitative manner it is rather evident that the a transition is likely to take place based on the balance of all three free energy contributions. In the current system this transition seems to take place at about 50% d-DMF where the interfacial tension is of the order of $\gamma = 14$–15 mN m^{-1}.

† In the absence of other contributions, the same interfacial energy implies a core radius exactly 50% bigger in spherical micelles as compared to cylindrical micelles. This can be understood by the following argument: the interfacial free energy scales like $F_{int} \sim 2\gamma/R_c^{cyl}$, $F_{int} \sim 3\gamma/R_c^{sphere}$, respectively. This implies that the equivalent radius in absence of any other contribution would be: $R_c^{cyl} = 2/3R_c^{sphere}$.

In order to quantitatively understand this transition and its stability range, it is interesting to compare with a thermodynamic model. A very detailed and accurate model was presented by Zhulina *et al.*[5] It should be mentioned however, that a comparison with a thermodynamical model in the present case is not straight forward for two reasons. First, available thermodynamical models for block copolymers (mean-field or scaling) use statistical properties of a chain to calculate the free energy terms which thus would need long chains. This is not strictly true for the present polymer which consists of only 17 PEP and 34 PEO repeat units. Secondly, the interactions in PEO systems are not trivial as aqueous solutions of PEO exhibit concentration and temperature dependent interaction parameters and a lower critical solution temperature solubility (LCST) behaviour (see *e.g.* ref. 41 and references therein). The situation might be even more complicated in the present d-DMF/D_2O mixed solvent system. The application of the model described in Section 2.1 may be considered as a first quantitative approach to describe the data. Further theoretical work would be necessary to obtain a more appropriate description of PEO and systems on the border between oligomers and polymers, but this is beyond the scope of this paper.

The calculations based on the equations given in Section 2.1 were performed using all constraints in terms of molecular parameters fixed. This included the molecular weights and compositions known from the chemical characterizations, the radii of gyration and segment lengths known from earlier SANS investigations[39,40] and interfacial tensions published in an earlier work.[29] After fixing the effective segment length of PEO[40] (l_{PEO} = 5.8 Å at 20 °C) and PEP[39] (l_{PEP} = 8.4 Å at 20 °C), only the prefactors involved in the corona free energy, C_H and C_F were allowed to vary in the fits. In order to take into account finite variations of the solvent quality of DMF–water with respect to PEO, we considered the scaling prediction by Zhulina *et al.*[5] ($C_H \sim A_2^{1/3}$) and write: $C_H = A_2(X_{DMF})/A_2(0)^{1/3}$. Based on the results given in ref. 29, it turns out that X_{DMF} can be related to γ in a simple exponential fashion find $A_2(X_{DMF})$ can be described by a parabola‡.

It was soon realized that whenever considering only the radii of the core, several solutions we found *i.e.* several pairs of C_H and C_F could describe the data. Therefore it also important to consider the thickness of the corona, D_{corona}, which within the theory of Zhulina *et al.*[5] also depends on C_H according to:

$$D_{corona} = \begin{cases} R_c \cdot \left[\left(1 + \frac{l_{PEO} C_H N_{PEO} \left(s l_{PEO}^{-2} \right)^{(\nu-1)/2\nu}}{\nu R_c} \right)^{\nu} - 1 \right] & \text{Spheres} \\ R_c \cdot \left[\left(1 + \frac{(1+\nu) \cdot l_{PEO} C_H N_{PEO} \left(s l_{PEO}^{-2} \right)^{(\nu-1)/2\nu}}{2\nu R_c} \right)^{2\nu/(1+\nu)} - 1 \right] & \text{Cylinders} \end{cases} \quad (16)$$

‡ These results published in ref. 29 are based on measurements of the interfacial tension towards PEP and A_2 virial coefficients in various water–DMF mixtures. To a very good approximation the quantities can be parameterized using: $A_2(X_{DMF}) = 2.6 - 6X_{DMF} + 4.6X_{DMF}^2$ and $X_{DMF} = 2.5 \exp^{-\gamma/9.13}$, where γ is in units of mN m^{-1} and $A_2(X_{DMF})$ is in units of 10^{-3} cm^3 mol/g^2. Using a combination of these two equations, we obtain a functional form of $A_2(\gamma)$ and consequently $C_H(\gamma)$ that can be inserted into the thermodynamic equations.

Here R_c obviously corresponds to the equilibrium value obtained by minimizing the whole expression for $F_{micelle}$ (eqn (1)). In order to obtain consistent results we therefore performed simultaneous fits of both R_c and D_{corona}. The fit results from the calculations for both cylindrical and spherical micelles are given in Fig. 5 showing the R_c and D_{corona} and the fit results for various interfacial tensions.

From the fits we obtain; $C_H = 0.21$ and $C_F = 2.04$ for spherical micelles and $C_H = 0.55$ and $C_F = 0.94$ for cylindrical micelles respectively. It should be pointed out that in the original theoretical work in ref. 5, these prefactors are not expected to depend on morphology. However, as pointed out in ref. 29 small variations in the solvent quality give rise to stronger effects within the block copolymer corona than for the homopolymer case. This might be related to the peculiar behavior of PEO[41] (hydrogen bonding and concentration dependent interaction parameters). Thus, it might be that these effects may affect the

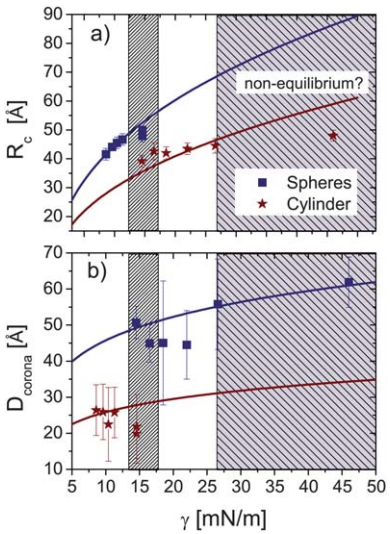

Fig. 5 Simultaneous fit of solution of thermodynamical model evaluated at its global minimum core radius to a) the core radius and b) the D_{corona} as a function of the interfacial tension for the two morphologies. The solid lines display the fit obtained by numerical solution and iterative fitting.

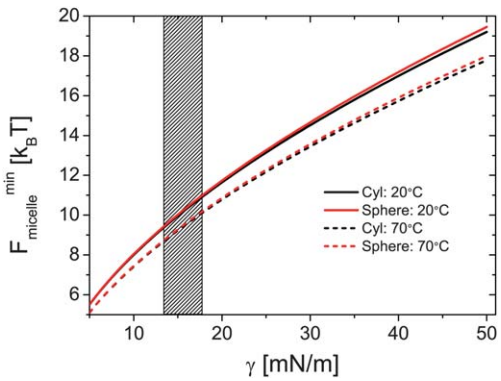

Fig. 6 Resulting free energy evaluated at the core radius corresponding to the minimum value of R_c, $F_{micelle}^{min}$.

prefactors C_H and C_F beyond what we can take into account using available data for the PEO homopolymer.

The resulting $F^{\min}_{\text{micelle}}$ evaluated at the minimum value for R_c for the two geometries are given in Fig. 6.

As seen from the results of the analysis, the model can rather satisfactorily describe the structural parameters obtained from the SANS data. In particular, the description is very good for the spherical micelles although some deviations are seen for the D_{corona} in both cases. Also for the cylindrical micelles, the fits show some discrepancy, especially at high interfacial tension. We will come back to this issue later.

Turning the attention to the values of the extracted $F^{\min}_{\text{micelle}}$, we see that the values for both morphologies are very close indicating that the system is close to the phase boundary. However the thermodynamical model gives an excellent consistency with the observed morphological behaviour of the system. At high interfacial tensions, $F^{\min}_{\text{micelle}}$ is clearly lower for the cylindrical micelles which are thus favoured in this range. This agrees very well with the experimental data where cylinder indeed are observed. This in principle also explains that the cylindrical micelles formed in water are also stable after thermal treatment at 70 °C. As depicted in Fig. 6, the calculations confirm that the relative stability of cylinders is unchanged at 70 °C§. At lower interfacial tensions, however, the line for $F^{\min}_{\text{micelle}}$ corresponding to the cylindrical micelles gradually approaches that of the spherical micelles. Above 10–15 mN m^{-1} the lines are indistinguishable suggesting that spherical micelles are also stable. This is in good accordance with the data where we observe a transition at about 15 mN m^{-1} (50% d-DMF). Here in this range, fluctuations may destabilize the cylindrical micelles further favouring spherical micelles. Such fluctuations have been shown to be important in morphological transitions in block copolymer melts.[21,42]

So far we have only considered equilibrium thermodynamics and disregarded the kinetic aspects. We believe that kinetic aspects and consequently non-equilibrium effects are prominent for high interfacial tensions (high water contents). It is highly probable that these effects are responsible for the strong deviations between experiment and theory at high interfacial tensions where the predicted line for cylindrical micelles is clearly higher than the experimental values for R_c in Fig. 5a). This is strongly supported by recent time resolved SANS experiments of a similar PEP1–PEO20/water–DMF system where unimer exchange was studied is several DMF–water mixtures. Here it was found that in pure water, no exchange was observed even on time scales of a day. In order to observe appreciable unimer exchange and consequently well-equilibrated micelles, the DMF concentration had to be raised to about 20–30%, *i.e.* $\gamma \approx$ 20–22 mN m^{-1}.[29] Hence comparing with the currently considered PEP1–PEO1 system which due to the smaller PEO block (1 kg/mole compared to 20 kg/mole) can be considered more "hydrophobic", we would not expect any significant exchange kinetics starting at DMF concentrations even higher than 20–30%. In fact, preliminary results from an ongoing study of the exchange kinetics in the current PEP1–PEO1/DMF–water show that the kinetics observed at 41% d-DMF occurs on a similar time scale (min–hours) as 30% in the other PEP1–PEO20 case.[26]

§ This is based on a rough calculation where we assume that prefactors are unchanged upon elevating the temperature

Hence coming back to our structural results, we do not expect to have micelles under proper thermodynamical equilibrium at d-DMF concentrations lower than at least about 30%. The absence of non-equilibrated micelles is in turn likely to be the main responsible factor for the strong deviation at high interfacial tensions between the equilibrium thermodynamical calculations and the experimental data in Fig. 5. In any case, it is interesting to note that also in pure D_2O the cylindrical morphology agrees with the theoretical calculations even though the chain exchange kinetics here is completely absent. Hence, while cylindrical micelles are more stable it is likely that these cannot reach their optimal size due to frozen or extremely retarded equilibrium kinetics. Now considering the path dependence of the structure of the micelles in 51% d-DMF, it is rather intriguing considering that the exchange kinetics are rather fast at this composition. The reason for this could be kinetic barriers involved in the transformation from spheres to cylinders. In addition the formation of spherical micelles has a low driving force due to the similarity of $F^{\min}_{\text{micelle}}$. It might also be that dynamic fluctuations in the corona further destabilize cylinders with respect to spheres. Once the transformation has occurred, the system will not readily go back to cylinders. This is in agreement with the findings of La Rue *et al.* who show that the sphere-to-cylinder transition is much slower than the opposite transition.[12] An effect that has also been seen in block copolymer melts and attributed to large entropic barrier associated with the merging of two spherical micelles into a cylindrical-like micelle.[21,42] In block copolymer solutions barriers are probably even larger because of stronger excluded volume interactions.

5 Conclusion

In this work we have shown that micelles formed by PEP1–PEO1/d-DMF/D_2O system undergo a morphological transition from cylinders to spheres at d-DMF contents of about 50%. By carefully mapping the system parameters to a detailed thermodynamic model, we have shown that the transition can be understood by the reduction of interfacial energy upon addition of d-DMF which is balanced by both core and coronal chain stretching. Whenever the interfacial tension is high, cylindrical micelles are favoured because of their smaller equivalent core radii (radius at equivalent interfacial energy) which thereby reduce the elastic energy of the chains in the core. At lower interfacial tensions, the system can afford a larger interfacial area which thus gives rise to smaller spherical micelles where the interchain repulsion in the corona is minimized.

The results from the comparison between the thermodynamic model and the structural data obtained from SANS show a quantitative description of the structural parameters. Interestingly, the resulting free energy profiles at the minimum values, reproduce the observed phase behaviour where cylindrical micelles are slightly more stable at high interfacial tensions. The experimentally found cross-over to spherical micelles also strongly agrees with the calculations where the spherical and cylindrical energies coincide. At high interfacial energies, we observe some deviation between experimental and theoretical results which we attribute to non-equilibrium structures as a results of slow exchange kinetics at these d-DMF/D_2O

compositions. These kinetic effects are also likely to further stabilize cylinders in water-rich solutions.

A comparison of results from parallel performed experiments on the exchange kinetics in this system additionally sheds some light on the thermodynamic potential and the importance of sample preparation. This is highlighted by comparing the thermal stability in pure water and 51% d-DMF. While in both cases cylinders are formed by direct dissolution, only the cylinders in water are stable upon thermal treatment. These systems differ by the chain exchange kinetics which are frozen in the former and fully active in 51% d-DMF. This behaviour can be attributed to the small difference in stability of cylindrical and spherical micelles in the 51% d-DMF solution. Hence despite the fast equilibration mechanism in terms of the exchange kinetics, cylindrical micelles remain stable due to the low driving force for spherical micelles. This is changed by increasing the temperature or increasing the DMF content which induces enough fluctuations to induce a morphological transition. The manner of which the micelles is formed from bulk and the control of their final size are thus likely to be embedded in the non-equilibrium dissolution process. A control of this process thus provides access to manipulate the properties of the micelles. This aspect in addition to the kinetics of morphological transitions, however, is outside the scope of this work and will be addressed in future publications.

Acknowledgements

The authors acknowledge the University of the Basque Country and Basque Country Government (Ref. No. IT-436-07, Depto. Educación, Universidades e InvestigaciónS, and iNANOGUNE research project within Etortek program) and the Spanish Minister of Education (Grant No. MAT 2007-63681) for their support. The support of the European Community within the SOFTCOMP Network of Excellence (NoE) program is also gratefully acknowledged.

References

1 I. W. Hamley *The Physics of Block Copolymers*, Oxford University Press, Oxford, UK 1998.
2 L. Leibler, H. Orland and J. C. Wheeler, *J. Chem. Phys.*, 1983, **79**, 3550–3557.
3 A. N. Semenov, *Sov. Phys. JETP*, 1985, **61**(4), 733–742.
4 R. Nagarajan and K. Ganesh, *J. Chem. Phys.*, 1989, **90**, 5843.
5 E. B. Zhulina, M. Adam, I. LaRue, S. S. Sheiko and M. Rubinstein, *Macromolecules*, 2005, **38**, 5330–5351.
6 S. Förster, U. Borchert, "Vesicles" in *Encyclopedia of Polymer Science and Technology*, 2005, 3rd Edition, Wiley, New York.
7 K. Yu, L. Zhang and A. Eisenberg, *Langmuir*, 1996, **12**, 5980–5984.
8 L. Zhang and A. Eisenberg, *Macromolecules*, 1999, **32**, 2239–2249.
9 Y. Zheng, Y. Y. Won, F. S. Bates, H. T. Davis, L. E. Scriven and Y. Talmon, *J. Phys. Chem. B*, 1999, **103**, 10331–5351.
10 L. Willner, A. Poppe, J. Allgaier, M. Monkenbusch, P. Lindner and D. Richter, *Europhys. Lett.*, 2000, **51**(6), 628.
11 H. Kaya, L. Willner, J. Allgaier, J. Stellbrink and D. Richter, *Appl. Phys. A*, 2002, **74**(Suppl.), S499–S501.
12 I. La Rue, M. Adam, M. Pitsikalis, N. Hadjichristidis, M. Rubinstein and S. S. Sheiko, *Macromolecules*, 2006, **39**, 309–314.
13 J. Bang, S. Jain, Z. Li, T. P. Lodge, J. S. Pedersen, E. Kesselman and Y. Talmon, *Macromolecules*, 2006, **39**, 1199–1208.
14 S. Abbas, Z. Li, H. Hassan and T. P. Lodge, *Macromolecules*, 2007, **40**, 4048–4052.
15 A. M. Mihut, M. Drechsler, M. Moeller and M. Ballauff, *Macromol. Rapid Commun.*, 2010, **31**(5), 449.
16 P. C. Hiemenz and R. Rajagopalan, "*Principles of Colloid and Surface Chemistry*", Marcel Dekker Inc., New York, 1997.
17 L. Leibler, *Macromolecules*, 1980, **13**, 1602.
18 F. S. Bates and G. H. Fredickson, *Annu. Rev. Phys. Chem.*, 1990, **41**, 525.
19 S. Sakurai, H. Kawada, T. Hashimoto and L. J. Fetters, *Macromolecules*, 1993, **26**, 5796.
20 S. Sakurai, T. Hashimoto and L. J. Fetters, *Macromolecules*, 1996, **29**, 740.
21 C. Y. Ryu, M. E. Vigild and T. P. Lodge, *Phys. Rev. Lett.*, 1998, **81**, 5354.
22 L. Willner, A. Poppe, J. Allgaier, M. Monkenbusch and D. Richter, *Europhys. Lett.*, 2001, **55**(5), 667.
23 R. Lund, L. Willner, J. Stellbrink, P. Lindner and D. Richter, *Phys. Rev. Lett.*, 2006, **96**, 068302.
24 R. Lund, L. Willner, E. E. Dormidontova and D. Richter, *Macromolecules*, 2006, **39**, 4566.
25 So. Choi, T. P. Lodge and F. S. Bates, *Phys. Rev. Lett.*, 2010, **104**, 047802.
26 R. Lund, L. Willner, J. Stellbrink, P. Lindner and D. Richter, *Phys. Rev. Lett.*, 2010, **104**, 049902.
27 R. Lund, L. Willner, M. Monkenbusch, P. Panine, T. Narayanan, J. Colmenero and D. Richter, *Phys. Rev. Lett.*, 2009, **102**, 188301.
28 R. Lund, L. Willner, A. Alegria, J. Colmenero and D. Richter, *Macromolecules*, 2008, **41**, 511.
29 R. Lund, L. Willner, J. Stellbrink, A. Radulescu and D. Richter, *Macromolecules*, 2004, **37**, 9984.
30 J. S. Pedersen and C. Svaneborg, *Curr. Opin. Colloid Interface Sci.*, 2002, **7**, 158–166.
31 J. S. Pedersen, C. Svaneborg, K. Almdal, I. W. Hamley and R. N. Young, *Macromolecules*, 2003, **36**, 416–433.
32 G. Beaucage, *J. Appl. Crystallogr.*, 1996, **29**, 134–46.
33 J. S. Pedersen, D. Posselt and K. Mortensen, *J. Appl. Crystallogr.*, 1990, **23**, 321–333.
34 C. Sommer, J. S. Pedersen and P. C. Stein, *J. Phys. Chem. B*, 2004, **108**, 6242–6249.
35 J. Allgaier, A. Poppe, L. Willner and D. Richter, *Macromolecules*, 1997, **30**(6), 1582–1586.
36 QtiKws is developed by Vitaliy Pipich at JCNS, Garching, Germany.
37 K. Devanand and J. C. Selser, *Macromolecules*, 1991, **25**, 5943–5947.
38 F. Tanaka, T. Koga and F. M. Winnik, *Phys. Rev. Lett.*, 2008, **101**, 028302.
39 D. Richter, M. Monkenbusch, A. Arbe and J. Colmenero, Nesutron Spin Echo in Polymer Systems, *Adv. Polym. Sci.*, 2005, **173**, Springer, Berlin, Germany.
40 B. Hammouda and D. L. Bo, *J. Polym. Sci., Part B: Polym. Phys.*, 2007, **45**(16), 2196.
41 E. E. Dormidontova, *Macromolecules*, 2002, **35**, 987.
42 F. M. Abuzaina, A. J. Patel, S. Mochrie, S. Narayanan, A. Sandy, B. A. Garetz and N. P. Balsara, *Macromolecules*, 2005, **38**, 7090.

